Article

Chinese Science Bulletin

Materials Science

February 2013 Vol.58 No.6: 689–695
doi: 10.1007/s11434-012-5456-9

Electrochemical performance of MCMB/(AC+$LiFePO_4$) lithium-ion capacitors

PING LiNa[1], ZHENG JiaMing[1], SHI ZhiQiang[2*], QI Jie[1]& WANG ChengYang[1*]

[1] *Key Laboratory for Green Chemical Technology of Ministry of Education, School of Chemical Engineering and Technology, Tianjin University, Tianjin 300072, China;*

[2] *Laboratory of Advanced Energy Materials and Devices, College of Materials Science and Engineering, Tianjin Key Laboratory of Fiber Modification and Functional Fiber, Tianjin Polytechnic University, Tianjin 300387, China*

Received February 28, 2012; accepted September 2, 2012

Lithium-ion capacitors (LICs) were fabricated using mesocarbon microbeads (MCMB) as a negative electrode and a mixture of activated carbon (AC) and $LiFePO_4$ as a positive electrode (abbreviated as LAC). The phase structure and morphology of LAC samples were characterized by X-ray diffraction (XRD) and field emission scanning electron microscopy (FESEM). The electrochemical performance of the LICs was studied using cyclic voltammetry, charge-discharge rate measurements, and cycle performance testing. A LIC with 30 wt% $LiFePO_4$ was found to have the best electrochemical performance with a specific energy density of 69.02 W h kg^{-1} remaining at 4 C rate after 100 cycles. Compared with an AC-only positive electrode system, the ratio of practical capacity to theoretical calculated capacity of the LICs was enhanced from 42.22% to 56.59%. It was proved that adding $LiFePO_4$ to AC electrodes not only increased the capacity of the positive electrode, but also improved the electrochemical performances of the whole LICs via Li^+ pre-doping.

lithium-ion capacitors, mesocarbon microbeads, activated carbon, $LiFePO_4$, Li^+ pre-doping

Citation: Ping L N, Zheng J M, Shi Z Q, et al. Electrochemical performance of MCMB/(AC+$LiFePO_4$) lithium-ion capacitors. Chin Sci Bull, 2013, 58: 689–695, doi: 10.1007/s11434-012-5456-9

With the dramatically rising demand for hybrid electric vehicles (HEVs) seen in recent decades, a challenge to discover novel electrochemical devices that possess both high power density and competitive energy density has emerged. Several strategies have been promoted [1–5]. One of these methods is combining the high specific power of the supercapacitors with the high specific energy of the batteries, named lithium-ion capacitors (LICs). Lithium-ion battery and capacitor electrode materials can be incorporated in serial or parallel at the internal level within one electrochemical cell. The most widely investigated approach is internal serial hybridization. Amatucci et al. [1] developed the first internal serial non-aqueous hybrid device using a Li^+ intercalation negative electrode based on $Li_4Ti_5O_{12}$, with activated carbon as an electrical double layer positive electrode. However, Cericola et al. [6] reported that parallel hybridization is superior to the serial approach. A bi-material electrode [7] consists of an electrode in which the charge is stored with different charging mechanisms (i.e. in the double layer and using a faradaic reaction). Pasquier et al. [8] built a $Li_4Ti_5O_{12}$/(AC+$LiCoO_2$) power-ion battery and discussed the effect of adding activated carbon to the positive electrode. In this report, $LiCoO_2$ was used as the positive electrode active material in combination with 5%–20% activated carbon. The device demonstrated good rate capability and a specific energy of 40 W h kg^{-1}. Hu et al. [9,10] reported hybrid battery-capacitors with $Li_4Ti_5O_{12}$ negative electrodes and $LiFePO_4$ or $LiMn_2O_4$ and activated carbon (AC) composite positive electrodes, where the amount of $LiMn_2O_4$ was varied between 15% and 30%. The specific energy of the resulting device varied from 9.8 to 11 W h kg^{-1}. However, these above mentioned hybrid batteries or capacitors could only be charged-discharged between 1.2 and 3.2 V or at lower potentials, because of the high elec-

*Corresponding authors (email: cywang@tju.edu.cn; shizhiqiang@tjpu.edu.cn)

trode potential of $Li_4Ti_5O_{12}$ (1.55 V versus Li).

In respect that graphite materials [11], the best choice for the negative electrode of lithium-ion batteries, can be intercalated by Li^+ at more negative potentials and are environment friendly, the graphite/AC LICs were also studied [4]. Still, employing graphite as negative electrode in LICs resulted in inevitable irreversible capacity loss (ICL) [11], which prevents the positive electrode from discharging fully [5], and leads to lower efficiency as well as poor electrochemical performance. As for activated carbon cathodes, the specific capacity is directly proportional to the surface area accessible to electrolytes. Current porous carbon materials have surface areas of about 1000–3500 m^2/g, with corresponding capacitances of less than 200 F/g in aqueous electrolytes and 100 F/g in organic electrolytes [12]. Therefore, the low capacity of AC hinders further improvement of energy density in LICs.

In order to solve these problems, we added Li^+ containing species into activated carbon (AC) electrodes. Because of reports that commonly available ACs [13] do not stay stable when charged to voltages as high as the electrode potential of $LiCoO_2$, $LiMn_2O_4$ or $LiNiO_2$ [14], we chose $LiFePO_4$ which exhibits a lower charge-discharge plateau than the others. Thus, in this paper, the effects of Li^+ addition on whole LICs electrochemical performance were investigated using composite electrode materials containing AC and $LiFePO_4$, hereafter abbreviated as LAC.

1 Experimental

1.1 Preparation of the electrodes

(i) Positive electrode. LAC composite material was prepared via a direct mixing technique. Different mass percentage (0, 10, 20 and 30 wt%) of $LiFePO_4$ (No.18, China Electronics Technology Group Corporation, capaticy: 138.4 mA h g^{-1} at 0.2 C) were added to activated carbon (AC, YP-D, Japan Kuraray Co. Ltd). The measured specific surface area and porosity parameters of the activated carbon are listed in Table 1. The mixture was then dispersed in distilled water (pH ca. 7) and stirred at 2000 r/min for 6 h to obtain the final LAC composite material. The stability of $LiFePO_4$ in water was investigated by Porcher et al. [15,16], who reported that $LiFePO_4$ slightly changed upon aging when it was brought in contact with water, and that the capacity of $LiFePO_4$ underwent no significant difference change after immersion in distilled water. According to their different $LiFePO_4$ contents of 0, 10, 20 and 30 wt%, the prepared LACs were marked as LAC0, LAC10, LAC20 and LAC30, respectively. Positive electrodes were prepared by mixing LAC composite material with polytetrafluoroethylene (PTFE) binder and carbon black (VXC72, Carbot Corp., USA) electrical conductor in a mass ratio of 82∶8∶10, after which the mixture was rolled into a film and pressed onto aluminum foil.

(ii) Negative electrode. Commercially available mesocarbon microbeads (MCMB, average particle size = 10 μm, graphitization temperature = 2800°C), were selected as the negative active electrode material. The MCMB was mixed with polyvinylidene fluoride (PVDF, dissolved in N-methyl-2-pyrrolidinone (NMP)) and carbon black (VXC72) in a mass ratio of 87∶7∶6 to form a slurry. After casting the slurry onto copper foil and evaporation of the NMP solvent at 80°C, the negative electrode was roll-pressed to enhance inter-particle contact and ensure better adhesion to the current collector.

1.2 Design and fabrication of cells

The LICs were assembled using the prepared MCMB (capacity: ca. 372 mA h g^{-1}, including 27 mA h g^{-1} of ICL) and LAC (capacity: shown in Table 2, at 2.0–3.8 V versus Li) as negative and positive electrodes, respectively. Theoretically, to achieve $Q_{LAC} = Q_{MCMB}$, the mass ratio of LAC/MCMB should be between 5/1 and 8/1, however, considering the compromise between energy and power, we selected a ratio of 2/1 in this study [4]. According to the different content of $LiFePO_4$ in the positive electrode, the series of LICs prepared were marked as MCMB/LAC0, MCMB/LAC10, MCMB/LAC20 and MCMB/LAC30. A 1 mol/L solution of $LiPF_6$ in 1/1 (v/v) ethylene carbonate/diethyl carbonate (EC/ DEC) mixture was used as electrolyte. Porous polypropylene microporous sheet (C2400, Celgard Corp., USA) was used as the separator. All the cells were fabricated in a glove box under a dry argon atmosphere.

1.3 Performance evaluation

Coin type cells (CR2430) were used for electrochemical performance tests. Cyclic voltammograms (CV) of the electrodes (AC, LAC20, $LiFePO_4$ and MCMB) were obtained using a three electrode cell, in which metallic Li was used as reference and counter electrodes, and a Princeton 2273 electrochemical workstation (USA). All other electrochemical testing was performed on an Arbin instrument (USA). A Micromeritics Tristar 3000 system was used for nitrogen adsorption/desorption measurements at 77 K. The phase structure of the samples was evaluated by X-ray diffraction

Table 1 Specific surface area and porosity parameters of activated carbon

Sample	$S_{BET}(N_2)$ (m^2 g^{-1})	S_{micro} [a] (m^2 g^{-1})	V_{tot} (m^3 g^{-1})	V_{micro} [a] (m^3 g^{-1})
AC	1507	1129	0.78	0.57

a) Obtained after applying the *t*-plot method to the N_2 adsorption data.

Table 2 Electrochemical performance of the LICs at 4*C* rate

Samples	$C^{a)}_{cal-positive}$ (mA h g^{-1})	$C^{b)}_{cal-capacitor}$ (mA h g^{-1})	$C^{c)}_{exp-capacitor}$ (mA h g^{-1})	$E^{d)}$ (W h kg^{-1})	$R^{e)}$ (%)
MCMB/LAC0	40.50	27.00	11.40	33.06	42.22
MCMB/LAC10	49.40	32.93	14.10	40.89	42.82
MCMB/LAC20	56.82	37.88	16.30	47.27	43.03
MCMB/LAC30	63.09	42.06	23.80	69.02	56.59

a) Theoretical specific capacity of positive electrode; b) theoretical specific capacity of LICs calculated for the total mass of two electrodes; c) practical specific capacity of LICs calculated for the total mass of two electrodes; d) specific energy density of LICs calculated for the total mass of two electrodes; e) ratio of practical capacity to theoretical calculated capacity.

(XRD) in the range $10°<2\theta<60°$ using a Rigaku Max 2500 diffractometer with Cu Kα radiation (λ = 0.154056 nm) at 40 kV and 200 mA. Field emission scanning electron microscopy (FESEM) was conducted using a Nano430 scanning electron microscope at 5 kV. All the measurements were carried out at room temperature, approximately 25°C.

2 Results and discussion

2.1 Structure and composition

The XRD patterns of $LiFePO_4$ and LAC composites with different $LiFePO_4$ contents are shown in Figure 1.

A typical diffraction pattern of non-graphitic carbon, featuring a characteristic broad 002 diffraction peak at 22.8° and a less intense peak at 43.4°, was obtained for LAC0. Apart from faint broad peaks attributed to non-graphitized carbon, only $LiFePO_4$ peaks (JCPDS card No. 81-1173, olivine type with orthorhombic lattice (*Pnma*) parameters: a=1.0332 nm, b=0.6010 nm, c=0.4692 nm) appeared in the patterns of all LAC samples. The intensity of the diffraction peaks gradually increased with the amount of $LiFePO_4$. These results indicate that no reaction occurred when AC and $LiFePO_4$ were mechanically mixed in distilled water, as reported by Porcher et al. [15, 16], because all diffraction peaks observed correspond to $LiFePO_4$ (JCPDS card No. 81-1173) and no additional crystallized phase was present.

Figure 2 shows FESEM images of $LiFePO_4$, AC, LAC10, LAC20 and LAC30 samples. Figure 2(a) shows a primary

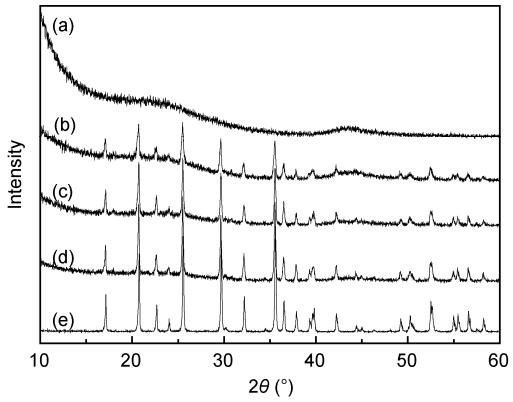

Figure 1 XRD patterns of the samples.

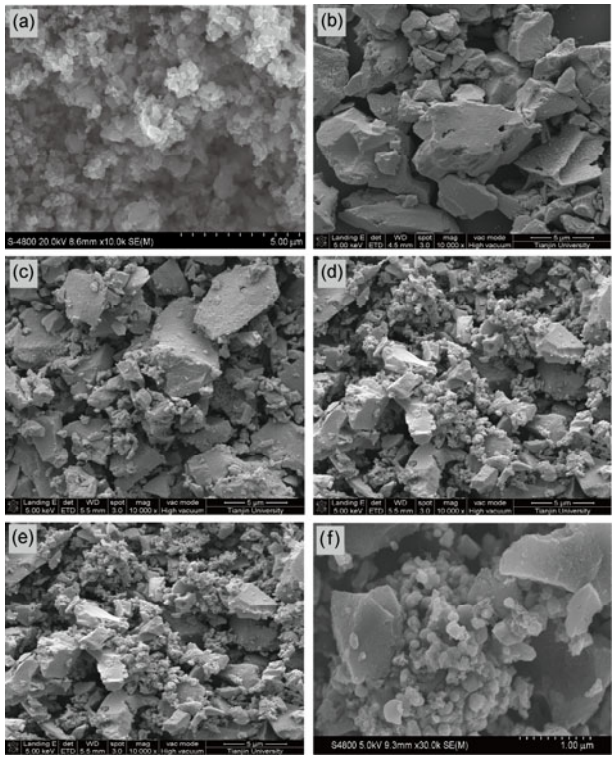

Figure 2 FESEM images of the samples. (a) $LiFePO_4$; (b) AC; (c) LAC10; (d) LAC20; (e) LAC30; (f) magnified view for LAC30.

$LiFePO_4$ crystallite size of 100–300 nm and an aggregate structure of 0.5–1 μm, indicating that the particles were mostly submicrometer. Figure 2(b) shows irregular AC particles with diameters of 3–10 μm. It can be seen from Figure 2(c)–(f) that the $LiFePO_4$ particles were uniformly dispersed at the surface of or between every AC particle. These images provide clear evidence that the two materials were well mixed and that the number of $LiFePO_4$ particles on the surface of the AC particles or between them increased with $LiFePO_4$ content.

2.2 Cyclic voltammetric behaviors of cells

The third cycle of the CV curves for the electrodes, MCMB/LAC0, MCMB/LAC20 and the MCMB/ $LiFePO_4$ battery are shown in Figure 3. Due to the cyclic voltammetric behaviors of samples MCMB/LAC10, MCMB/LAC20, and

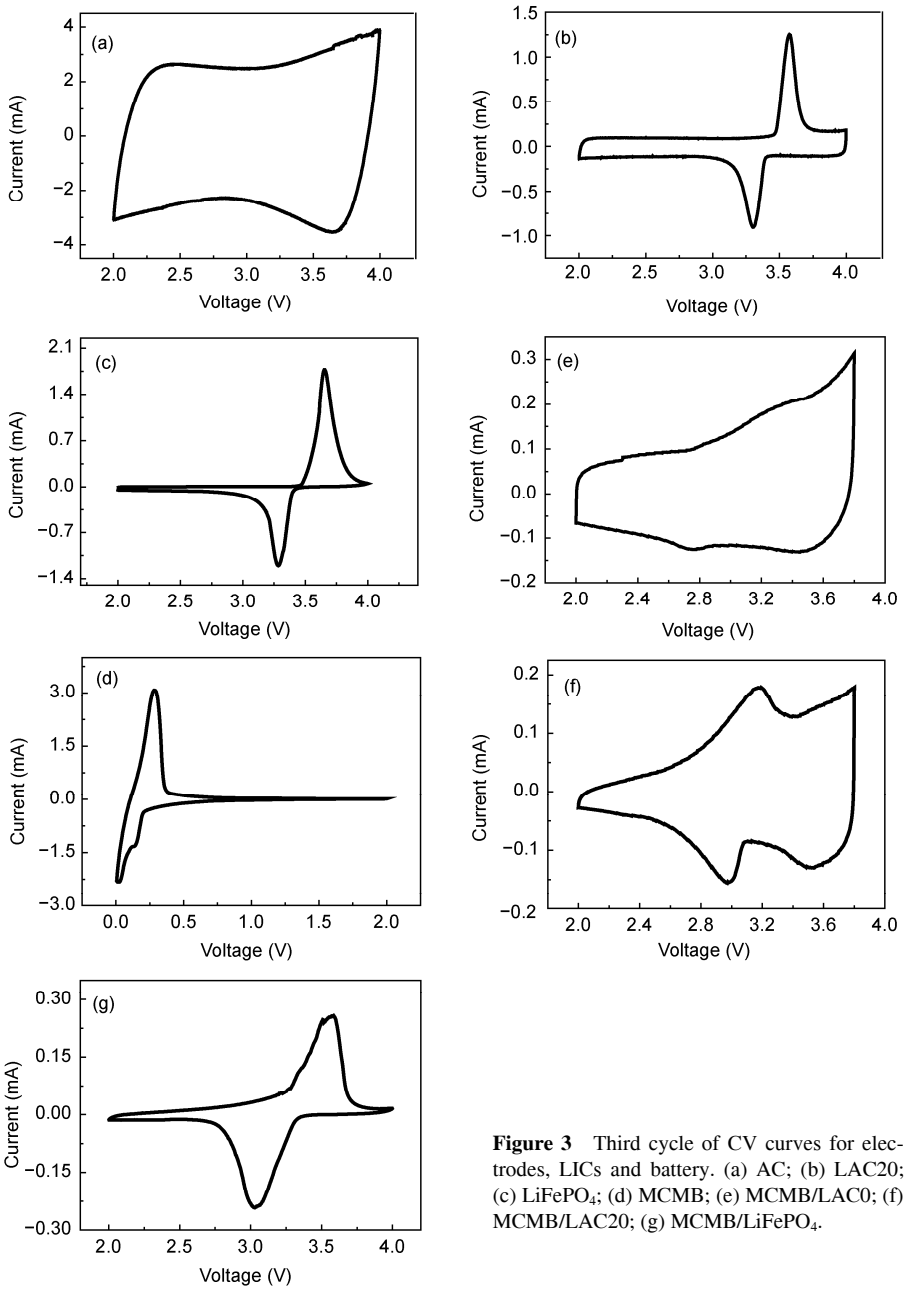

Figure 3 Third cycle of CV curves for electrodes, LICs and battery. (a) AC; (b) LAC20; (c) $LiFePO_4$; (d) MCMB; (e) MCMB/LAC0; (f) MCMB/LAC20; (g) MCMB/$LiFePO_4$.

MCMB/LAC30 being similar in appearance, only the CV curves of sample MCMB/LAC20 are shown in this paper. The voltage ranges were 0.005–2.0 V for the MCMB electrode, 2.0–3.8 V for the LICs, and 2.0–4.0 V for AC, LAC20, $LiFePO_4$ electrodes and MCMB/$LiFePO_4$ battery. The scan rates were 50 and 0.1 mV/s for AC electrode and MCMB/$LiFePO_4$ battery, respectively, and the scan rates for the other electrodes and LICs were 0.2 mV/s.

It is obvious that the AC, LAC20 and $LiFePO_4$ electrodes exhibited different electrochemical behaviors (Figure 3(a)–(c), respectively). In the range 2.0 to 4.0 V against Li metal, the near-mirror symmetry of the CV curve of the AC electrode is typical of double layer charging, attributed to the formation of a PF_6^- double layer on the surface of the AC electrode. The CV curve of the $LiFePO_4$ electrode shows oxidation-reduction behavior, i.e. Li^+ insertion-extraction reaction at the $LiFePO_4$ electrode, with a pair of redox peaks located at about 3.5 V. However, the LAC20 electrode exhibited two electrochemical behaviors: a double layer capacitance behavior (like AC electrode) and oxidation-reduction behavior (like $LiFePO_4$ electrode) in the corresponding potential range. The MCMB electrode also exhibited oxidation-reduction behavior, i.e. Li^+ insertion-extraction reaction at the $LiFePO_4$ electrode, a pair of redox peaks are located at about 0.2 V in Figure 3(d).

It can be seen from Figure 3(e)–(g) that the LICs and battery showed different electrochemical behaviors. The electrochemical behavior of sample MCMB/LAC0 (Figure

3(e)) is attributed to the combination of a Li^+ insertion-extraction reaction at the MCMB electrode and an interfacial anion adsorbing-desorbing process at the AC electrode, the CV curve is in accordance with typical double-layer capacitance behavior. This Li^+ insertion reaction is represented by a sharp oxidation peak at about 3.8 V. In contrast, the CV of the MCMB/$LiFePO_4$ battery system (Figure 3(g)) only shows oxidation-reduction peaks, i.e. Li^+ insertion-extraction reaction at MCMB and $LiFePO_4$ electrodes.

The electrochemical behavior of the MCMB/LAC20 system not only exhibited the double layer capacitance behavior of sample MCMB/LAC0, but also a symmetric pair of reduction-oxidation peaks at about 3.0 and 3.2 V Figure 3(f). It is evident that such redox peak response currents in the middle voltage range were caused by the $LiFePO_4$ component in the LAC composite material. The present CV results illustrate that $LiFePO_4$ and AC components in the LAC composite material brought respective charge storage ability into play over the whole working voltage range when a scan rate of 0.2 mV/s was used.

2.3 Galvanostatic charge-discharge behaviors of LICs

Figure 4 shows the galvanostatic charge-discharge profiles of (a) MCMB/LAC0 at a rate of 5*C* and (b) MCMB/LAC20 at different rate: 0.3*C*, 1*C*, 5*C* and 10*C*, at a working voltage range of 2.0–3.8 V. As shown in Figure 4(b), the whole charge-discharge process includes six steps (1–6) at 0.3*C* rate. In the charge process, the middle plateau (step 2) represents the process of Li^+ extraction from $LiFePO_4$. The typical linear voltage increase at the voltage range below or above 3.2 V (step 1, 3) is supposed to be the electrostatic adsorption of PF_6^- to AC. The discharge process is the reverse of the charge process. These results reveal that, over the whole working voltage range, there were two modes of energy storage in the sample MCMB/LAC20 system: Faradaic energy storage and electrostatic energy storage at 0.3*C* rate. This suggests that two electrochemical performances coexisted in this system, consistent with the cyclic voltammetric behavior shown in Figure 3(b). However, with increase current density the flat process vanishes, as shown in Figure 4(b), implying that the Faradaic energy storage weakened. The observed capacity attenuation was more intense from 0.3*C* to 1*C* than from 1*C* to 10*C*. Moreover, the charge-discharge profiles of MCMB/LAC20 at 5*C* and 10*C* rate were quite similar to the profile of sample MCMB/LAC0 shown in Figure 4(a), with a typically linear voltage increase over the whole voltage range, indicating that only electrostatic energy storage occured at high current density. The galvanostatic charge-discharge profiles of the MCMB/LAC10, MCMB/LAC20 and MCMB/LAC30 samples were similar.

2.4 Rate performance of the different LICs

Rate performances of the LICs containing AC with different added weight percents of $LiFePO_4$ as the positive electrode and MCMB as the negative electrode are presented in Figure 5.

Nearly no capacity loss is noticed during 10 cycles of charge-discharge at high rates ranging from 2*C* to 10*C*. These results demonstrate that the LICs with different $LiFePO_4$ content exhibited good performances at high charge-discharge rates, indicating that the present preparation method of the composite cathode materials provided high rate LIC charge-discharge performance. It can be seen that sample MCMB/LAC30 showed the best rate performance and capacity characteristics among all the samples, with specific discharge capacity of 18.4 mA h g^{-1} at a rate of 10*C*, and 73% retention of capacity compared with its capacity at a rate of 2*C*. Despite the fact that the capacity retentions of MCMB/LAC20, MCMB/LAC10 and MCMB/LAC0 were clearly higher than MCMB/LAC30, the specific discharge capacities of these samples decreased to lower values: 13.40, 12.00 and 10.60 mA h g^{-1}, respectively, when the rate was increased to 10*C*.

2.5 Cycle life performance of LICs

The cycle performances of the LICs in the potential range 2.0–3.8 V at 4*C* rate are shown in Figure 6.

The LIC charge-discharge model adopted for the first

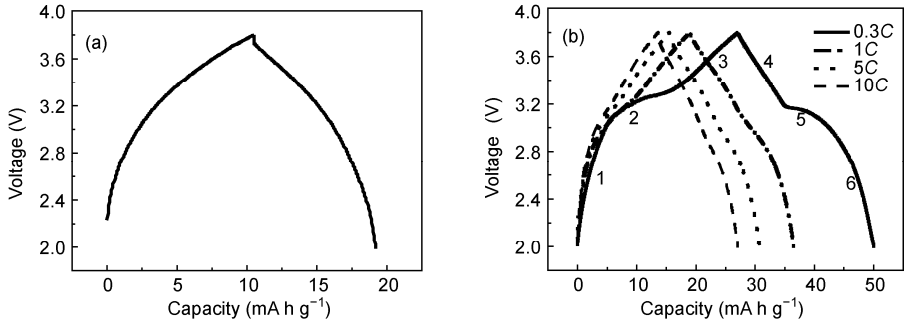

Figure 4 Galvanostatic charge-discharge profiles of the LICs. Specific capacities were calculated using total mass of two LIC electrodes. (a) MCMB/LAC0 5*C*; (b) MCMB/LAC20 0.3*C*, 1*C*, 5*C*, 10*C*.

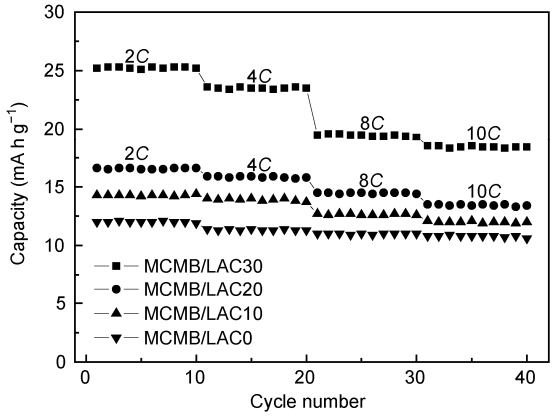

Figure 5 Specific discharge capacity of the LICs at different rates. Specific capacities were calculated using total mass of two LIC electrodes.

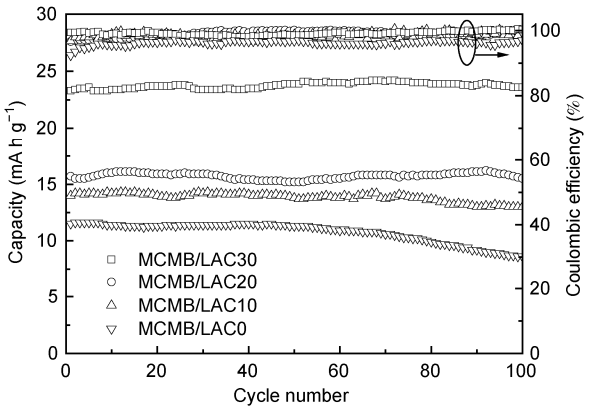

Figure 6 Specific discharge capacity and coulombic efficiency vs. cycle number of the LICs at 4*C* rate. Specific capacities were calculated using total mass of two LIC electrodes.

cycle was follows: the LICs were first charged at a current density of 0.1*C* up to a given voltage and then allowed to relax at open circuit for two hours. As the given voltage value was set higher, this repeated several times until the maximum working voltage was reached, after which the LICs were discharged at a rate of 4*C*. As shown in Figure 6, the coulombic efficiencies of MCMB/LAC10, MCMB/LAC20 and MCMB/LAC30 were close to 100%, which was more desirable than MCMB/LAC0 (95%). There was negligible specific capacity loss for both MCMB/LAC30 and MCMB/LAC20 after 100 cycles, while 25.20% and 7.14% specific capacity losses were observed for MCMB/LAC0 and MCMB/LAC10, respectively. The results confirm that the cycle performance of LICs was improved by Li^+ addition.

Table 2 shows the results of the electrochemical performance of different LICs at a rate of 4*C*. The specific capacity and specific energy density of the LICs were estimated based on the total mass of the two electrodes. $C_{\text{cal-positive}}$ and $C_{\text{cal-capacitor}}$ were calculated based on the assumption that the LICs take full advantage of the working potential flat of MCMB negative electrode (lower than 0.2 V versus Li), and the potential range of the positive electrode was 2.0-3.8 V. The theoretical specific capacity of the positive electrode can be calculated according to eq. (1) [17]

$$C_{\text{cal-positive}} = \frac{m_1 c_1 + m_2 c_2}{m_1 + m_2}, \quad (1)$$

where C_1 is the specific capacity of AC (C_1=40.5 mAh/g, 2.0–3.8 V versus Li), C_2 is the specific capacity of $LiFePO_4$ (C_2 =138.4 mA h g^{-1}), and m_1 and m_2 are the respective mass percentage of the two materials. The theoretical specific capacity of the LICs can be calculated according to eq. (2)

$$C_{\text{cal-capacitor}} = \frac{2}{3} C_{\text{cal-positive}}. \quad (2)$$

The specific energy density of the LICs can be calculated according to eq. (3) [18]

$$E = C_{\text{exp-capacitor}} \left(V_1^2 - V_2^2 \right), \quad (3)$$

where V_1 and V_2 equal to 3.8 and 2.0 V, respectively.

The specific energy densities of the LICs at $LiFePO_4$ mass percentages in the LAC composite material of 0, 10, 20 and 30 wt% were 33.06, 40.89, 47.27 and 69.02 W h kg^{-1}, respectively. It is notable that as the content of $LiFePO_4$ increased, the specific energy density of the LICs improved and reached a maximum 69.02 W h kg^{-1} at 30 wt%.

In order to investigate the effect of $LiFePO_4$ on the whole LICs, we defined a utilization rate parameter calculated according to eq. (4)

$$R = \frac{C_{\text{exp-capacitor}}}{C_{\text{cal-capacitor}}}. \quad (4)$$

The utilization rate of the LICs was enhanced to 56.59% in MCMB/LAC30 from 42.22% in MCMB/LAC0. The reason for this may be the following: adding of a Li^+ containing compound to the AC electrode compensated the irreversible capacity and reduced the working potential plateau of the MCMB electrode, allowing the positive electrode to discharge fully.

When the active carbon positive electrode is highly polarized, the adsorbed water and functional groups on the activated carbon surface contribute to the generation of H^+ at the positive electrode, and HF is produced by the reaction between PF_6^- and H^+. HF then reacts with SEI on the surface of the negative electrode and forms a porous structure (LiF). The surface of the negative electrode is thereby constantly directly exposed to the electrolyte, leading to continuous decomposition of the electrolyte [13]. The voltage of the LICs is the difference between the potentials of the positive and negative electrodes (U=(E^+)–(E^-)). The addition of Li^+ to the AC electrode reduced the working potential plateau of MCMB electrode, resulting in the maximum potential of the AC positive electrode of MCMB/LAC10 (or 20, 30) sample being lower than that of MCMB/LAC0, as

well as reductions in the level of polarization at the AC positive electrode and decomposition of electrolyte on the negative electrode. Furthermore, adding a Li^+ containing compound to LICs also compensates for Li^+ consumption by generating LiF. As described above, the specific discharge capacity and coulombic efficiency vs. cycle number of LICs are improved when using LACs as the positive electrode, as shown in Figure 6. The effect is equivalent to the negative electrode lithium pre-doping process in previously hybrid electrochemical capacitors [5,19,20,21].

3 Conclusions

The electrochemical performance of LICs, including specific energy density, cycle life and coulombic efficiency were improved by adding proportions of $LiFePO_4$ into AC positive electrode. The discharge specific capacity of the LICs increased remarkably with $LiFePO_4$ content despite a slight decrease in rate performance. Among the series of LICs fabricated, MCMB/LAC30 exhibited the best electrochemical performance. Its specific energy density remained 69.02 W h/kg after 100 cycles when the current density was 4 C rate. Moreover, its utilization ratio (practical capacity to theoretical calculated capacity) was enhanced to 56.59% from 42.22% for the system without Li^+ addition.

This work was supported by the National Natural Science Foundation of China (*51172160, 50902102*)*, the National High Technology Research and Development Program of China* (*2011AA11A232*)*, and the National Basic Research Program of China* (*2012CB720302*).

1 Amatucci G G, Badway F, Pasquier A D, et al. An asymmetric hybrid nonaqueous energy storage cell. J Electrochem Soc, 2001, 148: A930–A939
2 Naoi K, Ishimoto S, Isobe Y, et al. High rate nano crystalline $Li_4Ti_5O_{12}$ attached on carbon nano-fibers for hybrid supercapacitors. J Power Sources, 2010, 195: 6250–6254
3 Conway B E, Pell W G. Double-layer and pseudo-capacitance types of electrochemical capacitors and their applications to the development of hybrid devices. J Solid State Electrochem, 2003, 7: 637–644
4 Khomenko V, Raymundo-Piñero E, Béguin F. High-energy density graphite capacitor in organic electrolyte. J Power Sources, 2008, 177: 643–651
5 Aida T, Yamada K, Morita M. An Advanced Hybrid Electrochemical capacitor that uses a wide potential range at the positive electrode. Electrochem Solid-State Lett, 2006, 9: A534–A536
6 Cericola D, Novák P, Wokaun A, et al. Hybridization of electrochemical capacitors and rechargeable batteries: An experimental analysis of the different possible approaches utilizing activated carbon, $Li_4Ti_5O_{12}$ and $LiMn_2O_4$. J Power Sources, 2011, 196: 10305–10313
7 Cericola D, Novák P, Wokaun A, et al. Segmented bi-material electrodes of activated carbon and $LiMn_2O_4$ for electrochemical hybrid storage devices: Effect of mass ratio and C-rate on current sharing. Electrochimica Acta, 2011, 56: 1288–1293
8 Pasquier A D, Plitz I, Gural J, et al. Power-ion battery: Bridging the gap between Li-ion and supercapacitor chemistries. J Power Sources, 2004, 136: 160–170
9 Hu X B, Huai Y J, Lin Z J, et al. A ($LiFePO_4$-AC)/$Li_4Ti_5O_{12}$ hybrid battery capacitor. J Electrochem Soc, 2007, 154: A1026–A1030
10 Hu X B, Lin Z J, Liu L, et al. Effects of the $LiFePO_4$ content and the preparation method on the properties of ($LiFePO_4$+AC)/$Li_4Ti_5O_{12}$ hybrid battery-capacitors. J Serb Chem Soc, 2010, 75: 1259–1269
11 Shi H, Barker J, Koksbang R. Structure and lithium intercalation properties of synthetic and natural graphite. J Electrochem Soc, 1996, 143: 3466–3472
12 Bose S, Kuila T, Mishra A K. Carbon-based nanostructured materials and their composites as supercapacitor electrodes. J Mater Chem, 2012, 22: 767–784
13 Aida T, Murayama I, Yamada K, et al. Analyses of capacity loss and improvement of cycle performance for a high-voltage hybrid electrochemical capacitor. J Electrochem Soc, 2007, 154: A798–A804
14 Tarascon J M, Armand M. Issues and challenges facing rechargeable lithium batteries. Nature, 2001, 414: 359–367
15 Porcher W, Moreau P, Lestriez B, et al. Is $LiFePO_4$ stable in water? Toward greener Li-ion batteries. Electrochem Solid—State Lett, 2008, 11: A4–A8
16 Porcher W, Moreau P, Lestriez B, et al. Stability of $LiFePO_4$ in water and consequence on the Li battery behavior. Ionics, 2008, 14: 583–587
17 Pico F, Ibanez J, Centeno T A, et al. $RuO_2{\cdot}xH_2O$/NiO composites as electrodes for electrochemical capacitors: Effect of the RuO_2 content and the thermal treatment on the specific capacitance. Electrochim Acta, 2006, 51: 4693–4700
18 Wang H Y, Masaki Y. Graphite, a suitable positive electrode material for high-energy electrochemical capacitors. Electrochem Commun, 2006, 8: 1481–1486
19 Sivakkumar S R, Pandolfo A G. Evaluation of lithium-ion capacitors assembled with pre-lithiated graphite anode and activated carbon cathode. Electrochimica Acta, 2012, 65: 280–287
20 Fujii T, Hatozaki O. Electric storage device and its production method. US Patent. S 20100255356 A1, 2010-10-07
21 Ping L N, Zheng J M, Shi Z Q, et al. Electrochemical performance of lithium ion capacitors using Li^+-intercalated mesocarbon microbeads as the negative electrode. Acta Phys-Chim Sin, 2012, 28: 1733–1738